ARMY RESEARCH LABORATORY

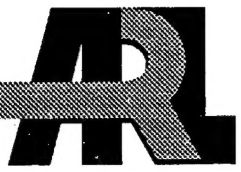

Computational Modeling of Sense and Destroy Armor (SADARM) Submunition Separation/Collision

by Jubaraj Sahu, Karen R. Heavey,
and Charles J. Nietubicz

ARL-TR-1378 June 1997

The findings in this report are not to be construed as an official Department of the Army position unless so designated by other authorized documents.

Citation of manufacturer's or trade names does not constitute an official endorsement or approval of the use thereof.

Destroy this report when it is no longer need. Do not return it to the originator.

Army Research Laboratory
Aberdeen Proving Ground, MD 21005-5066

ARL-TR-1378 **June 1997**

Computational Modeling of Sense and Destroy Armor (SADARM) Submunition Separation/Collision

Jubaraj Sahu, Karen R. Heavey, Charles J. Nietubicz
Weapons and Materials Research Directorate, ARL

Abstract

Sense and Destroy Armor (SADARM) is a high-priority Army program that experienced an initial design flaw, leading to submunition collisions. Computational fluid dynamics (CFD), including Chimera overset technology, has recently been applied to solve this problem. The CFD modeling has provided significant physical insight into the complex unsteady flow field associated with the SADARM submunitions during the separation/ejection process. CFD simulations have predicted that, with the addition of the fins on the trailing submunition, separation will occur, and collisions will be avoided.

ACKNOWLEDGMENTS

A conceptual and scientific visualization video was developed and produced by Ms. Deborah Thompson and Mr. Erik Mark of the High Performance Computing Division, Corporate Information and Computing (CICC), U.S. Army Research Laboratory-Aberdeen Proving Ground (ARL-APG). Their work was essential in providing a clean description of the problem and its relationship to the computational fluid dynamics (CFD) results and is most gratefully acknowledged.

INTENTIONALLY LEFT BLANK.

TABLE OF CONTENTS

INTENTIONALLY LEFT BLANK.

LIST OF FIGURES

INTENTIONALLY LEFT BLANK.

1. INTRODUCTION

An important parameter in the design of shell and bodies flying in relative motion to each other is the total aerodynamic drag. The base drag constitutes a large part of the total aerodynamic drag, and accurate prediction of the base region flow field is necessary. The ability to compute the base-region flow field for projectile configurations using Navier-Stokes computational techniques has been developed over the past several years [1, 2]. Recently, improved numerical predictions have been obtained using a more advanced zonal upwind flux-split algorithm [3]. This zonal scheme preserves the base corner, which allows an accurate modeling of the base-region flow. Previous computational studies have been completed showing the aerodynamic effect for a variety of base geometries. These calculations, however, were performed on stand-alone projectile configurations and represent a single-body problem. Recently, a multibody problem that involves other bodies flying in the wake of a parent projectile has required computational analyses [4]. This is due in part to the difficulty in finding good experimental and/or analytical data for such problems. The particular problem here was to determine the aerodynamic effect of small cylindrical segments being ejected into the wake of a parent projectile. The complexity and uniqueness of this problem resulted from the trailing segments being in relative motion to each other, embedded in a nonuniform wake flow, and requiring a time-dependent solution. These calculations were performed at a supersonic speed for the dynamic case, which involved time-accurate numerical computations, and the computed results were found to be in good agreement with the test data.

The present problem is another multibody problem that involves separation of two submunitions at a low transonic speed. The Sense and Destroy Armor (SADARM) program is a high-priority Army program that had experienced an initial design flaw leading to submunition collisions. Figure 1 shows the components for the initial system. Separation of the submunitions depends on the initial ejection velocity. For small initial ejection or separation velocity, the submunitions can in fact separate initially, but later in the flight are pulled back together to collide. Figure 2 shows the collision of two submunitions in a flight test. A time-accurate

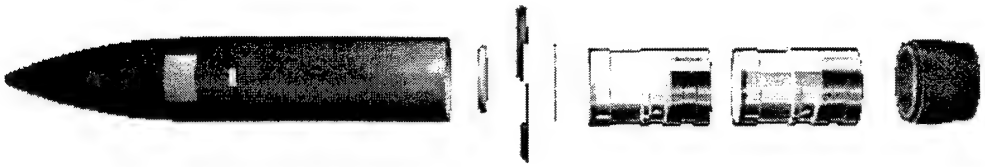

Figure 1. Original SADARM projectile design.

Figure 2. Collisions of two submunitions in flight.

numerical solution of this problem is the subject matter of this research report, intended to provide more basic flow-field information and understanding to avoid such collisions.

The time accurate numerical simulation of the multiple aerodynamic bodies in relative motion has been obtained using the Chimera [5] approach. This technique has been used to compute inviscid and viscous flows about complex configurations [6, 7], and has been demonstrated for unsteady viscous-flow problems with bodies in relative motion [8]. The Chimera approach is a domain decomposition method that uses overset, body-conforming grids and grew out of the necessity to computationally model geometrically complex configurations. The originally developed Navier-Stokes numerical capability, zonal F3D [3], was extended by the authors to include the details of the Chimera procedure. This work couples the solution of the Navier-Stokes equations, which govern fluid motion, with the solution to the 6 degree-of-freedom (DOF) equations of motion. The coupling of the fluid-dynamic solution and rigid-body motion eliminates the need for simplifying assumptions and allows more accurate physically based simulations.

2. GOVERNING EQUATIONS AND SOLUTION TECHNIQUE

The complete set of time-dependent, Reynolds-averaged, thin-layer Navier-Stokes equations is solved numerically to obtain a solution to this problem. The numerical technique used is an implicit, finite-difference scheme. Time-accurate calculations are made to numerically simulate the separation and collision of two submunitions.

2.1 Governing Equations. The complete set of three-dimensional (3-D), time-dependent, generalized geometry, Reynolds-averaged, thin-layer Navier-Stokes equations for general spatial coordinates ξ, η, and ζ can be written as follows [9]:

$$\partial_\tau \hat{q} + \partial_\xi \hat{F} + \partial_\eta \hat{G} + \partial_\zeta \hat{H} = Re^{-1} \partial_\zeta \hat{S}, \tag{1}$$

where

$\xi = \xi(x, y, z, t)$ - longitudinal coordinate;
$\eta = \eta(x, y, z, t)$ - circumferential coordinate;
$\zeta = \zeta(x, y, z, t)$ - nearly normal coordinate;
$\tau = t$ - time

and

$$\hat{q} = \frac{1}{J}\begin{bmatrix} \rho \\ \rho u \\ \rho v \\ \rho w \\ e \end{bmatrix} \qquad \hat{F} = \frac{1}{J}\begin{bmatrix} \rho U \\ \rho u U + \xi_x p \\ \rho v U + \xi_y p \\ \rho w U + \xi_z p \\ (e+p)U - \xi_t p \end{bmatrix}$$

$$\hat{G} = \frac{1}{J}\begin{bmatrix} \rho V \\ \rho u V + \eta_x p \\ \rho v V + \eta_y p \\ \rho w V + \eta_z p \\ (e+p)V - \eta_t p \end{bmatrix} \qquad \hat{H} = \frac{1}{J}\begin{bmatrix} \rho W \\ \rho u W + \zeta_x p \\ \rho v W + \zeta_y p \\ \rho w W + \zeta_z p \\ (e+p)W - \zeta_t p \end{bmatrix} \tag{2}$$

and where

$$\hat{S} = \frac{1}{J}\begin{bmatrix} 0 \\ \mu(\zeta_x^2 + \zeta_y^2 + \zeta_z^2)u_\zeta + \frac{\mu}{3}(\zeta_x u_\zeta + \zeta_y v_\zeta + \zeta_z w_\zeta)\zeta_x \\ \mu(\zeta_x^2 + \zeta_y^2 + \zeta_z^2)v_\zeta + \frac{\mu}{3}(\zeta_x u_\zeta + \zeta_y v_\zeta + \zeta_z w_\zeta)\zeta_y \\ \mu(\zeta_x^2 + \zeta_y^2 + \zeta_z^2)w_\zeta + \frac{\mu}{3}(\zeta_x u_\zeta + \zeta_y v_\zeta + \zeta_z w_\zeta)\zeta_z \\ \left\{ (\zeta_x^2 + \zeta_y^2 + \zeta_z^2)\left[\frac{\mu}{2}(u^2 + v^2 + w^2)_\zeta + \frac{\kappa a_\zeta^2}{Pr(\gamma - 1)}\right] \right. \\ \left. + \frac{\mu}{3}(\zeta_x u + \zeta_y v + \zeta_z w)(\zeta_x u_\zeta + \zeta_y v_\xi + \zeta_z w_\zeta) \right\} \end{bmatrix}. \tag{3}$$

In Equation 1, the thin-layer approximation is used, and the viscous terms involving velocity gradients in both the longitudinal and circumferential directions are neglected. The viscous terms are retained in the normal direction, ζ, for the projectile and segments, and are collected into the vector $\hat{S}$. In the wake or the base region, similar viscous terms are also added in the streamwise direction, ξ. For this computation, the diffusion coefficients μ and κ contain molecular and turbulent parts. The turbulent contributions are supplied through an algebraic eddy viscosity turbulence model developed by Baldwin and Lomax [10].

The velocities in the ξ, η, and ζ coordinate directions can be written as

$$U = \xi_t + u\xi_x + v\xi_y + w\xi_z$$
$$V = \eta_t + u\eta_x + v\eta_y + w\eta_z$$
$$W = \zeta_t + u\zeta_x + v\zeta_y + w\zeta_z,$$

which represent the contravariant velocity components.

The Cartesian velocity components (u, v, w) are retained as the dependent variables and are nondimensionalized with respect to a_∞ (the free-stream speed of sound). The local pressure is determined using the relation

$$p = (\gamma - 1)[e - 0.5\rho(u^2 + v^2 + w^2)], \tag{4}$$

where γ is the ratio of specific heats. Density, ρ, is referenced to ρ_∞ and the total energy, e, to $\rho_\infty a_\infty^2$. The transport coefficients are also nondimensionalized with respect to the corresponding free-stream variables. Thus the Prandtl number that appears in $\hat{S}$ is defined as $Pr = c_{p\infty}\mu_\infty/\kappa_\infty$.

2.2 Numerical Technique. The implicit, approximately factored scheme for the thin-layer Navier-Stokes equations using central differencing in the η and ζ directions and upwinding in ξ is written in the following form [11],

$$\left[I + i_b h\delta_\xi^b(\hat{A}^+)^n + i_b h\delta_\zeta \hat{C}^n - i_b h Re^{-1}\bar{\delta}_\zeta J^{-1}\hat{M}^n J - i_b D_i|_\zeta\right]$$

$$\times\left[I + i_b h\delta_\xi^f(\hat{A}^-)^n + i_b h\delta_\eta \hat{B}^n - i_b D_i|_\eta\right]\Delta\hat{Q}^n$$

$$= -i_b\Delta t\left\{\delta_\xi^b\left[(\hat{F}^+)^n - \hat{F}_\infty^+\right] + \delta_\xi^f\left[(\hat{F}^-)^n - \hat{F}_\infty^-\right] + \delta_\eta\left(\hat{G}^n - \hat{G}_\infty\right)\right.$$

$$\left. + \delta_\zeta\left(\hat{H}^n - \hat{H}_\infty\right) - Re^{-1}\bar{\delta}_\zeta\left(\hat{S}^n - \hat{S}_\infty\right)\right\} - i_b D_e\left(\hat{Q}^n - \hat{Q}_\infty\right), \qquad (5)$$

where $h = \Delta t$ and the free-stream base solution is used. Here, δ is typically a three-point second-order accurate central difference operator, $\bar{\delta}$ is a midpoint operator used with the viscous terms, and the operators δ_ξ^b and δ_ξ^f are backward and forward three-point difference operators. The flux $\hat{F}$ has been eigensplit, and the matrices $\hat{A}$, $\hat{B}$, $\hat{C}$, and $\hat{M}$ result from local linearization of the fluxes about the previous time level. Here, J denotes the Jacobian of the coordinate transformation. Dissipation operators D_e and D_i are used in the central space differencing directions. The smoothing terms used in the present study are of the form:

$$D_e|_\eta = (\Delta t)J^{-1}\left[\epsilon_2\bar{\delta}\rho(B)\beta\bar{\delta} + \epsilon_4\bar{\delta}\frac{\rho(B)}{1+\beta}\bar{\delta}^3\right]|_\eta J$$

$$D_i|_\eta = (\Delta t)J^{-1}\left[\epsilon_2\bar{\delta}\rho(B)\beta\bar{\delta} + 2.5\epsilon_4\bar{\delta}\rho(B)\bar{\delta}\right]|_\eta J,$$

where

$$\beta = \frac{|\bar{\delta}^2 P|}{|(1+\delta^2)P|}$$

and where $\rho(B)$ is the true spectral radius of B. The idea here is that the fourth difference will be tuned down near shocks (e.g., as β gets large, the weight on the fourth difference drops down while the second difference tunes up).

2.3 Chimera Composite Grid Scheme. The Chimera overset grid scheme is a domain decomposition approach where a configuration is meshed using a collection of overset grids. It allows each component of the configuration to be gridded separately and overset into a main grid. Overset grids are not required to join in any special way. Usually there is a major grid that covers the entire domain or a grid generated about a dominant body. Minor grids are generated about the rest of the other bodies. Because each component grid is generated independently, portions of one grid may be found to lie within the solid boundary contained within another grid. Such points lie outside the computational domain and are excluded from the solution process.

In the submunition separation problem, the first (leading) submunition is a major grid and the second (trailing) submunition grid is a minor grid. The minor grid is completely overlapped by the major grid; thus, its outer boundary can obtain information by interpolation from the major grid. Similar data transfer or communication is needed from the minor grid to the major grid. However, a natural outer boundary that overlaps the two submunition grids does not exist. The Chimera technique creates an artificial boundary (also known as a hole boundary) between grids that provides the required path for information transfer from the first submunition to the second. The resulting hole region is excluded from the flow-field solution in the projectile grid. Equation 5 has been modified for Chimera overset grids by the introduction of the flag i_b to achieve just that. This i_b array accommodates the possibility of having arbitrary holes in the grid. The i_b array is defined such that $i_b = 1$ at normal grid points and $i_b = 0$ at hole points. Thus, when $i_b = 1$, equation 5 becomes the standard scheme. But, when $i_b = 0$, the algorithm reduces to $\Delta\hat{Q}^n = 0$ or $\hat{Q}^{n+1} = \hat{Q}^n$, leaving $\hat{Q}$ unchanged at hole points. The set of grid points that form the border between the hole points and the normal field points are called intergrid boundary points. These points are updated by interpolating the solution from the overset grid that created the hole. Values of the i_b array and the interpolation coefficients needed for this update are provided by a separate algorithm [6].

In the present study, which involves multiple bodies in relative motion, the location of the holes and the intergrid boundary points are time dependent. Accordingly, the i_b array and the interpolation coefficients are functions of time. This procedure of unsteady Chimera

decomposition has been successfully demonstrated by Meakin [8]. The method depends on three functions: domain connectivity, aerodynamics, and body dynamics. The aerodynamics code depends on the domain connectivity code to supply hole and interpolation information. The domain connectivity code, in turn, depends on the body dynamics code to supply the location and orientation of the moving bodies relative to the primary body. Finally, the body dynamics code depends on the aerodynamics code to provide the aerodynamic forces and moments acting on the moving bodies.

The Chimera procedure reduces a complex multibody problem into a number of simpler subproblems. For moving-body problems, all grids are allowed to move with 6 DOF relative to an inertial reference frame. Accordingly, bodies can move with respect to others without the necessity of generating new grids. With this composite overset grid approach, it is thus possible to determine the unsteady relative motion of the segments and associated aerodynamic forces without the need for costly regridding. This also eliminates potential accuracy problems due to severe grid stretching used by many other techniques. The solution procedure is to compute the flow field at each time step; integrate the pressure and viscous forces for the trailing segments to obtain the drag force; use the predicted drag in a coupled 6-DOF program to compute the new relative position of the trailing segment. Because this is an axisymmetric calculation (0° angle of attack), only the drag coefficient is used to determine the motion of the segments. At the next time step, the solution procedure is repeated for the new position with the domain decomposition providing all the required interpolation information. Computations are performed on each grid separately. These grids use the available core memory one grid at a time. The remaining grids are stored on an external disk storage device such as the solid-state disk (SSD) device of the Cray C-90 or Y-MP computer.

2.4 Domain Connectivity Function. A major part of the Chimera overset grid approach is the information transfer from one grid into another by means of the intergrid boundary points. Again, these points consist of a set of points that define the hole boundaries and outer boundaries of the minor grids. These points depend on the solutions in the overlapping regions. In the present work, the Domain Connectivity Function in 3-D (DCF3D) Code [8] has been used to

establish the linkages between the various grids that are required by the flow solver or aerodynamics code described earlier. These include the determination of the interpolation coefficients and the setting up of Chimera logic for bodies making holes in overlapping grids. For unsteady moving-grid cases, this code must be executed at each time iteration. To minimize the computation time, this code uses the knowledge of hole and interpolated boundary points at time level n to limit its search regions for finding their corresponding locations at time level n+1.

In general, each component grid in an overset grid system represents a curvilinear system of points. However, the positions of all points in all the grids are defined relative to an inertial system of reference. To provide domain connectivity, inverse mappings are used that allow easy conversion from the x, y, z inertial system to ξ, ζ, η computational space. For moving-body problems, these maps for component grids are created only once. Identification of the intergrid boundary points that correspond to the outer boundaries of the minor grids is done simply by specifying appropriate ranges of coordinate indices. The rest of the intergrid boundary points that result from holes created by a body in overset grids is a little more difficult to identify. A collection of analytical shapes such as cones, cylinders, and boxes are used to cut holes in this method.

2.5 Boundary Conditions. For simplicity, most of the boundary conditions have been imposed explicitly [3]. An adiabatic wall boundary condition is used on the body surface, and the no-slip boundary condition is used at the wall. The pressure at the wall is calculated by solving a combined momentum equation. Free-stream boundary conditions are used at the inflow boundary as well as at the outer boundary. A symmetry boundary condition is imposed at the circumferential edges of the grid, while a simple extrapolation is used at the downstream boundary. A combination of symmetry and extrapolation boundary conditions is used at the center line (axis). Since the free-stream flow is supersonic, a nonreflection boundary condition is used at the outer boundary. Similar boundary conditions are used for the segments.

3. MODEL GEOMETRY AND COMPUTATIONAL GRID

Each submunition is a right circular cylinder of length-to-diameter ratio 1.38. Figure 3 shows an expanded view of a composite computational grid for these submunitions. The complete grid consists of approximately 102,660 grid points and is split into 8 sections. The grid in the wake region of each submunition consists of a large number of points in both the streamwise and normal directions. The surface points for each region (body and wake) are selected using an interactive design program. Each grid section was obtained separately and then appended to provide the full grid. The grid for the body region as well as the wake region was obtained algebraically. A body-conforming grid was obtained for each submunition and then overset to form the composite mesh shown in Figure 3. This case corresponds to the matted position when both submunitions are merged together (flying as one body). The major grid corresponds to the grid for the first submunition, which is easily generated independently of the minor grid (grid for the second submunition). The Chimera technique, as stated earlier, allows individual grids to be generated with any grid topology, thus making the grid generation process easier. For moving- body problems, both major and minor grids shown in Figure 3 in the matted position move with the submunitions as they separate from each other. Figure 4 is a grid at another instant in time when the minor grid has moved downstream into the wake of the major grid. Again, there is no need to generate new grids for the submunitions (minor and major) during the dynamic process.

4. RESULTS

Time-accurate calculations have been performed to numerically simulate the separation of two submunitions, both being in relative motion. All computations were run at $M_\infty = 0.80$ and $\alpha = 0°$, and atmospheric flight conditions were used. These calculations required 15M words of memory, and each case used about 20 hours of computer time on the Cray C-90 supercomputer. In order to numerically determine the submunition separation/collision process, computations were performed for several different initial separation velocities. Results are shown first for a

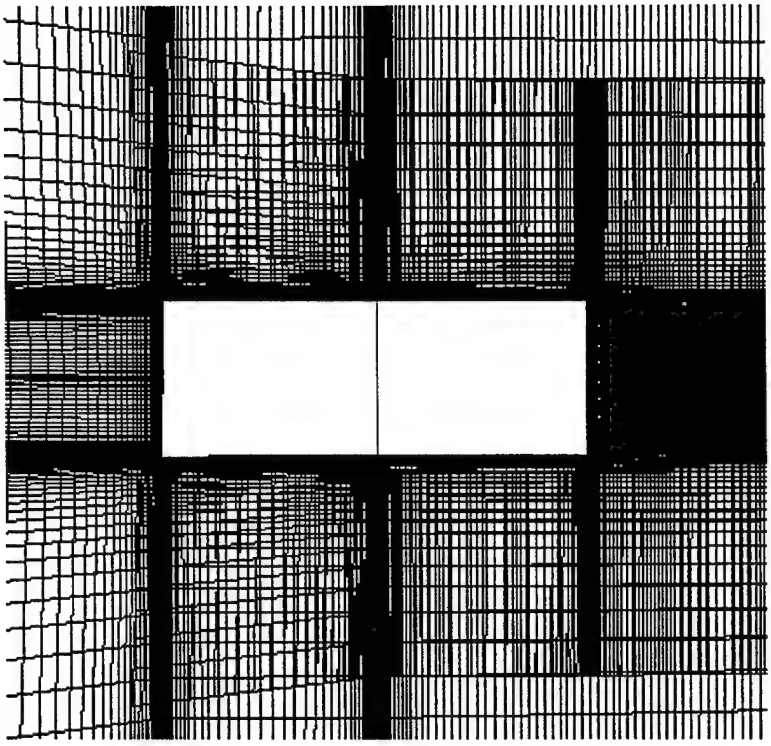

Figure 3. Composite grid (matted position).

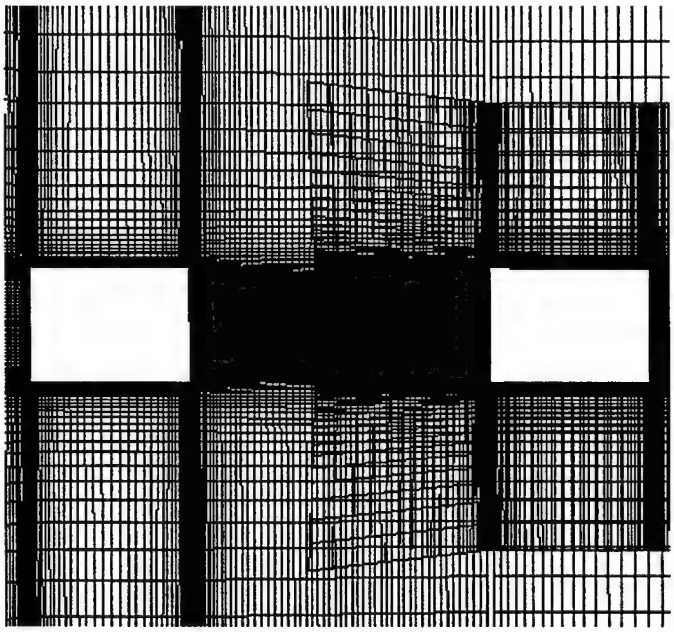

Figure 4. Composite grid (submunitions separated).

case where the initial separation velocity is 5 ft/s. Figure 5 shows the Mach number contours for the submunitions at three points in time: 9, 19.5, and 33.8 ms after separation began. As seen in this figure, the flow field is unsteady and the second submunition is completely submerged in the wake of the first submunition. The second submunition initially separates with the separation distance having increased in the time interval from 9.0 ms to 19.5 ms. Soon afterward, both submunitions pull back toward each other with the separation smaller at 33.3 ms than at 9.0 ms. The time-dependent numerical solution simulates the motion of both submunitions, and the aerodynamic drag changes continually (see Figure 6). Surface pressures including the base pressures and the viscous stresses are known from the computed flow field and are integrated to give the aerodynamic drag for both cylindrical submunitions. The drag coefficient for the submunitions is shown in Figure 6 as a function of the separation distance. This drag coefficient is based on the cross-sectional area of the submunition and the free-stream dynamic pressure. As mentioned earlier, the second submunition is submerged in the subsonic wake of the first submunition. The pressure behind the second submunition is higher than the pressure ahead of it and, therefore, results in negative drag. The fluctuating drag for both submunitions indicates that the flow field is unsteady. The drag for the first submunition is positive, which tends to slow its motion. The drag for the second submunition is negative, which leads to it being pulled back towards the first submunition. As seen in this figure, the separation distance increases to about 0.8 inches and then decreases. When both submunitions come back close to each other, the drags for these submunitions are found to be different from what they were during the initial separation. This is due to the fact that the flow field experienced by the submunitions during these processes are different. The drag contributions for each of the submunition surfaces (front, back, and top) are shown in the next two figures. In Figure 7, both the front and the back surfaces of the first submunition are contributors, although the front surface is shown to be the significant contributor to the drag. Figure 8 shows the drag from the second submunition is mainly from the front surface. For both submunitions, the top surfaces have little impact on the total drag. Figure 9 shows the separation distance as a function of time for the initial separation velocity of 5 ft/s. As seen here, the separation distance increases with time until a peak is reached at about 20 ms. The separation distance is clearly seen to decrease from that point on, and the two submunitions come back together and collide at 38 ms.

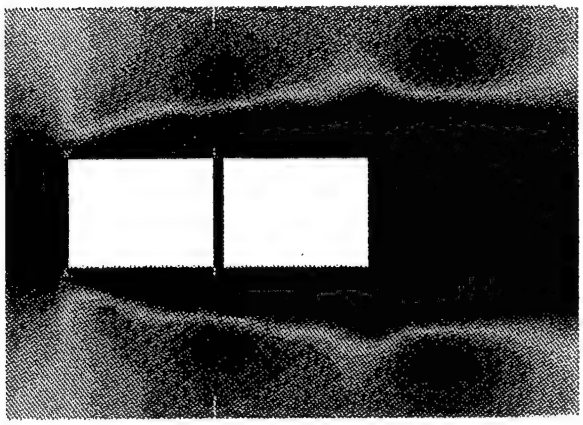

Time = 9.0 ms

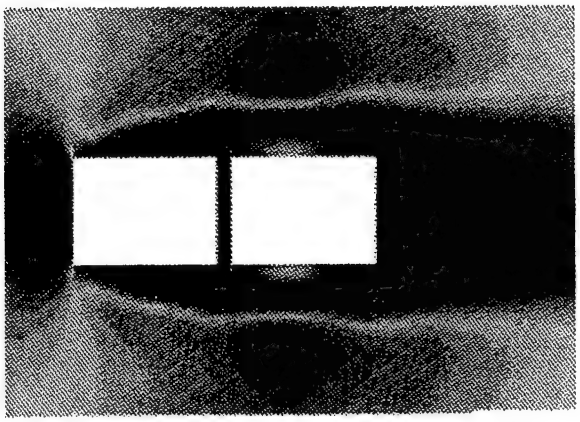

Time = 19.5 ms

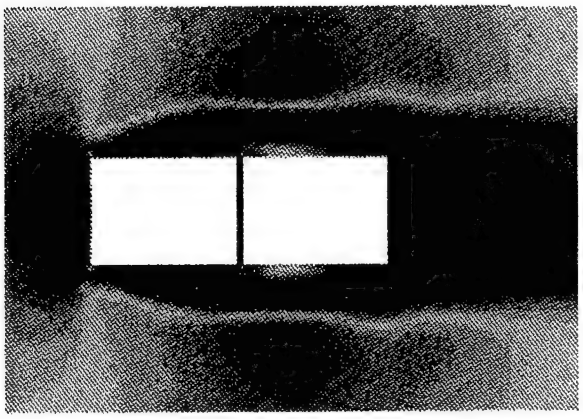

Time = 33.8 ms

Figure 5. Mach contours, M = .80, α = 0, V_s = 5 ft/s.

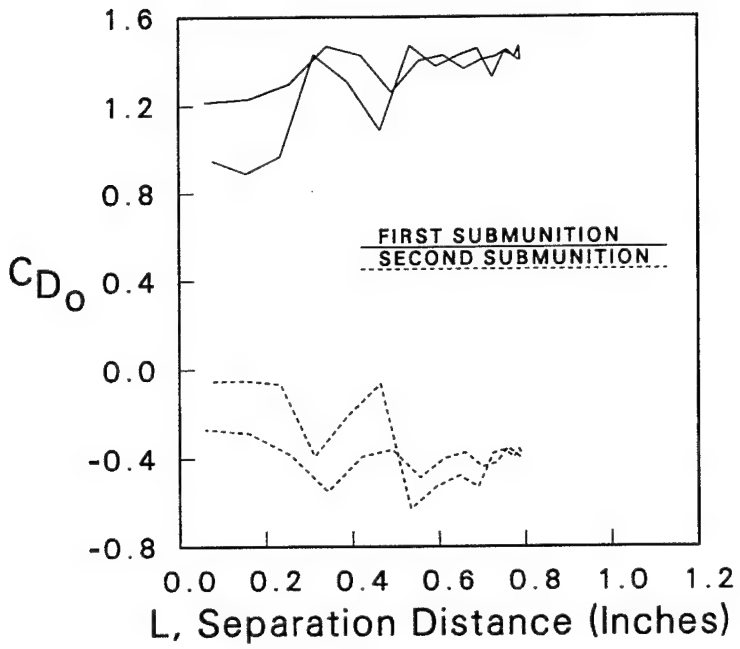

Figure 6. Drag coefficient, M = 0.80, α = 0, V_s = 5 ft/s .

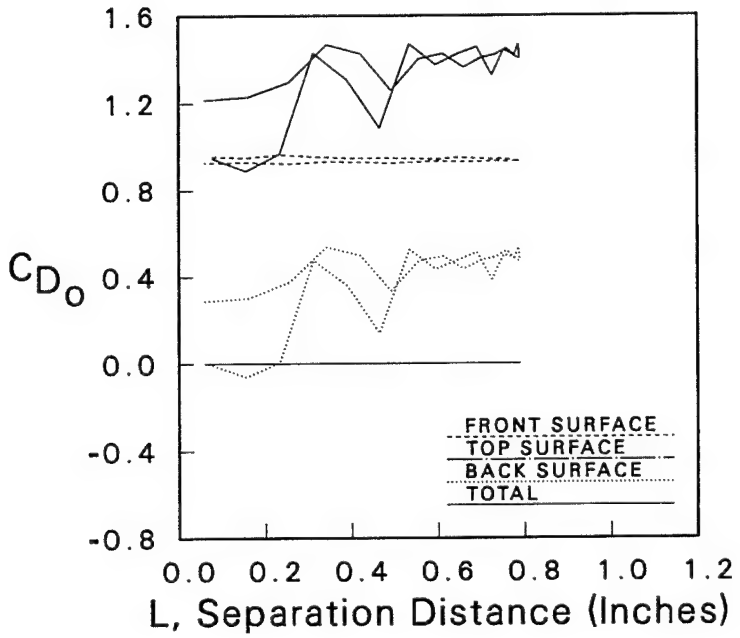

Figure 7. Drag coefficient, M = .80, α = 0, V_s = 5 ft/s (first submunition).

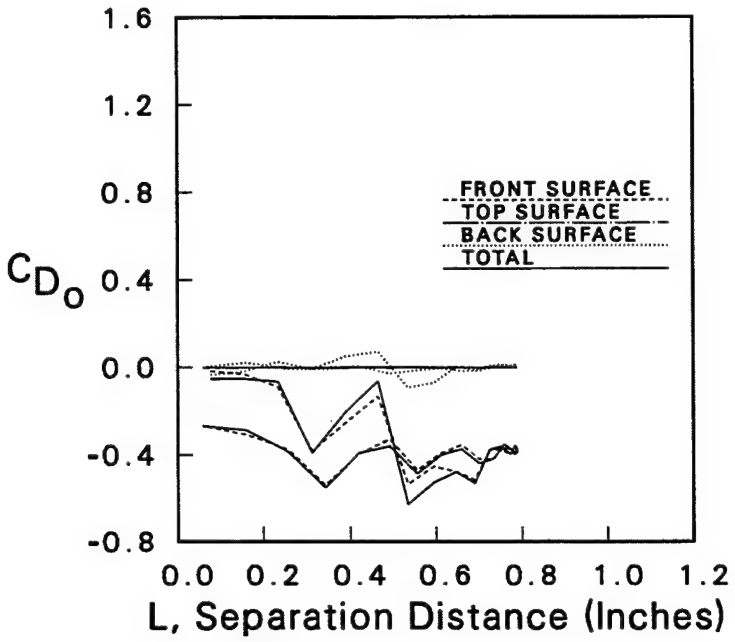

Figure 8. Drag coefficient, M = 0.80, $\alpha = 0$, $V_s = 5$ ft/s (second submunition).

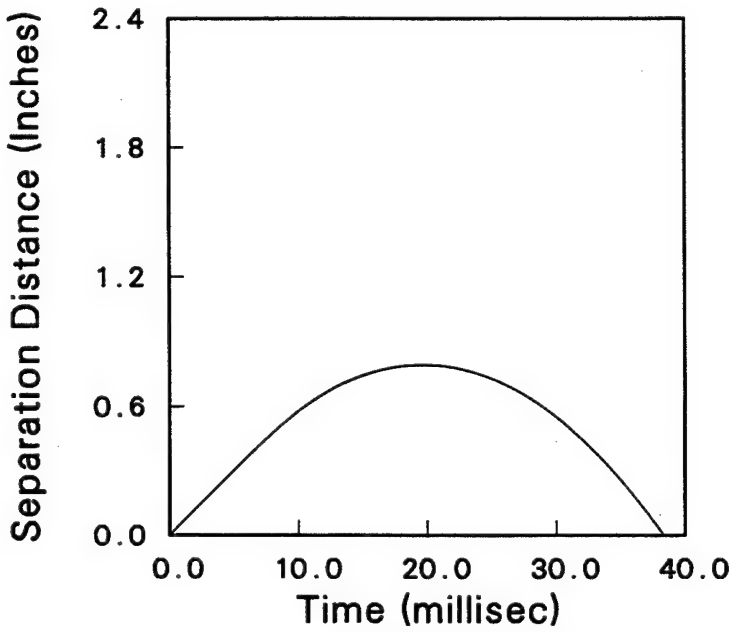

Figure 9. Separation distance vs. time, M = 0.80, $\alpha = 0$, $V_s = 5$ ft/s.

Initially, the calculations for the above case were done using a time interval of 0.01, using about 50 hours of central processing unit (CPU) time. A second computation was performed using a value of 0.03 for the time interval. This calculation used approximately 20 CPU hours. Figure 10 shows that the drag histories for both calculations are similar and reach the same separation distance before being pulled back towards each other. Similarly, Figure 11 shows the peak separation distance for both submunitions to be identical, and the time of collision is very similar. Based on these findings, the remainder of the calculations were done using the larger time interval of 0.03, providing a savings of over 50% of CPU time.

A modification to the projectile design resulted in an increase in the separation velocity. Consequently, a new set of calculations were performed, this time with an initial separation velocity of 15 ft/s. Figure 12 shows the Mach number contours for the submunitions at three points in time: 9, 41, and 69 ms after the onset of separation. The separation/collision process follows the same trend as demonstrated by the 5-ft/s case, with the submunitions initially separating. Again, as shown in Figure 13, the drag for the first submunition is positive, slowing its motion while the negative drag of the second submunition pulls it back towards the first submunition. After approximately 40 ms, the peak separation distance of 4 inches is reached and then the second submunition is pulled back toward the first submunition. Figure 14 clearly shows that collision occurs at 80 ms.

To avoid the submunition collision, it was thus necessary to either increase the initial separation velocity or incorporate devices such as fins to the second submunition to provide added drag. Because of system constraints, the initial separation velocity could not exceed 15 ft/s. Thus, the second option was selected and studied both numerically and experimentally. Figure 15 shows the improved projectile design. Fins were added to the second submunition as well as to the base plug, thus providing extra drag. A computational model of a finned submunition requires a 3-D calculation and large amounts of computer time and resources. Because of time constraints, the existing computer model was modified by adding extra drag to simulate fin-induced drag. The amount of added drag, as well as the time in which the drag devices deployed, was obtained from an experiment conducted on the submunition alone. The

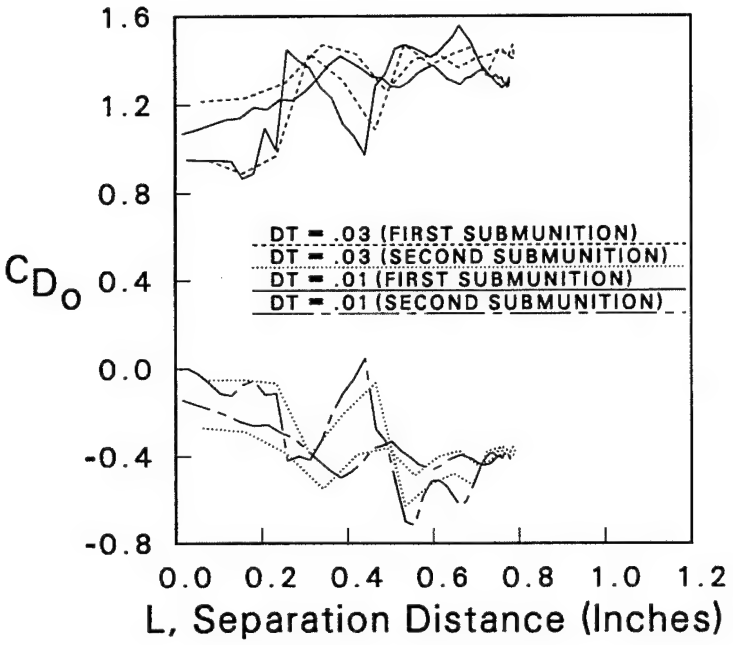

Figure 10. Total drag for two submunitions, M = 0.80, α = 0, V_s = 5 ft/s, Dt = 0.01, and 0.03.

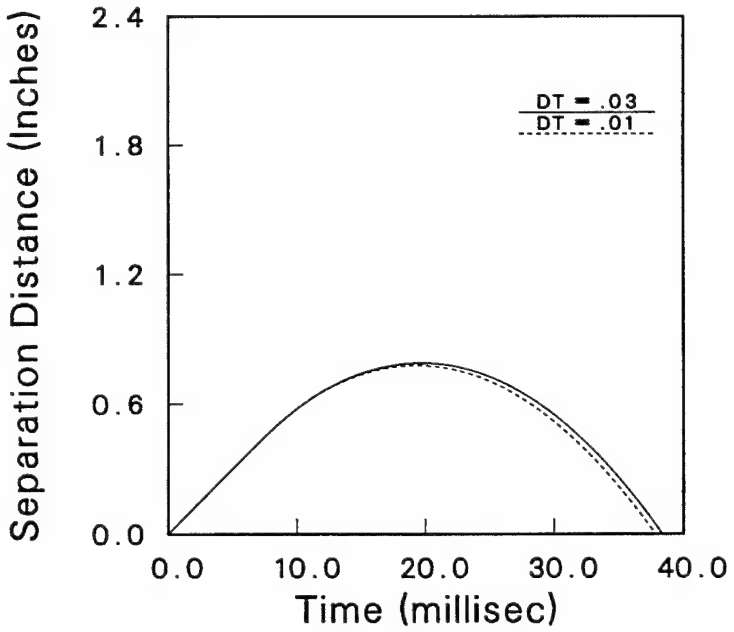

Figure 11. Separation distance vs. time, M = 0.80, α = 0, V_s = 5 ft/s, Dt = 0.01, and 0.03.

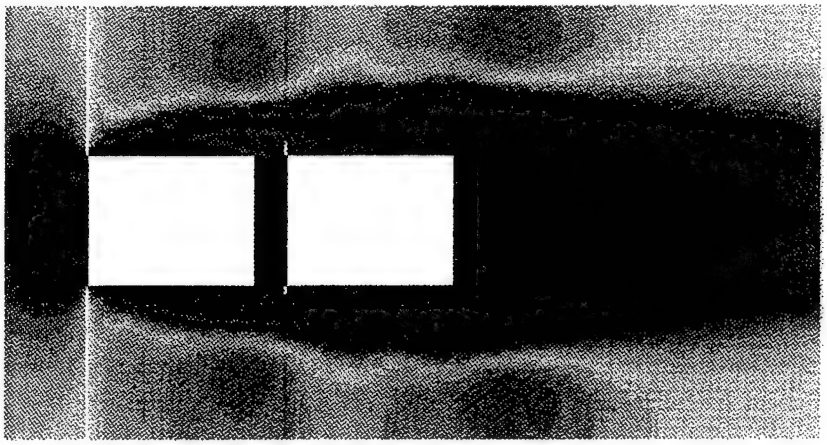

Time = 9.1 ms

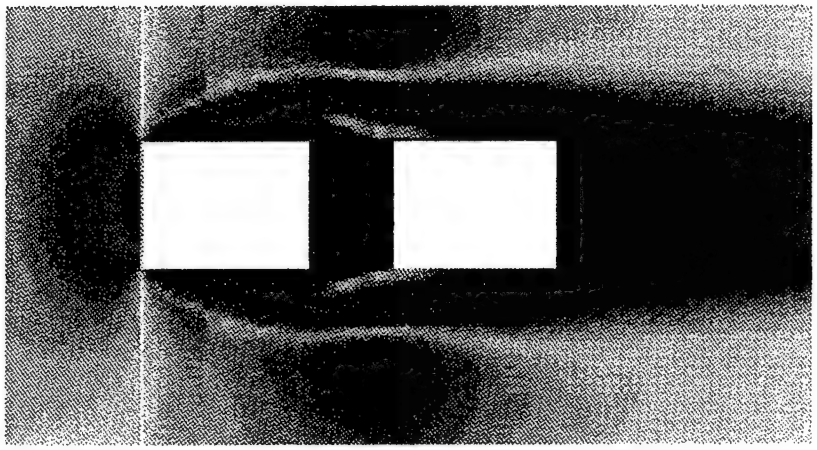

Time = 41.5 ms

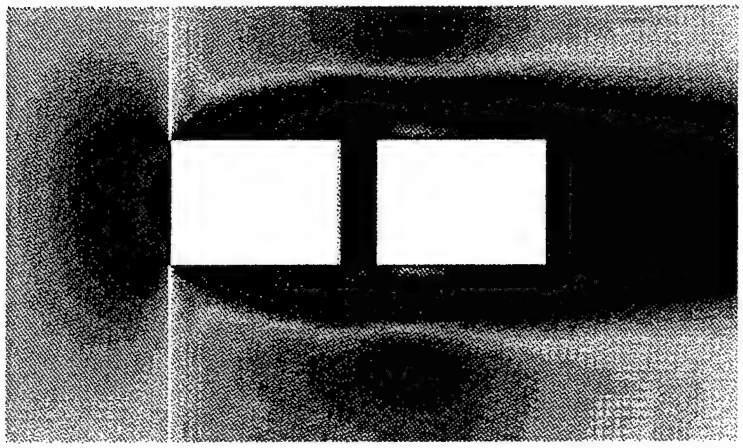

Time = 68.8 ms

Figure 12. Mach contours, M = .80, α = 0, V_s = 15 ft/s.

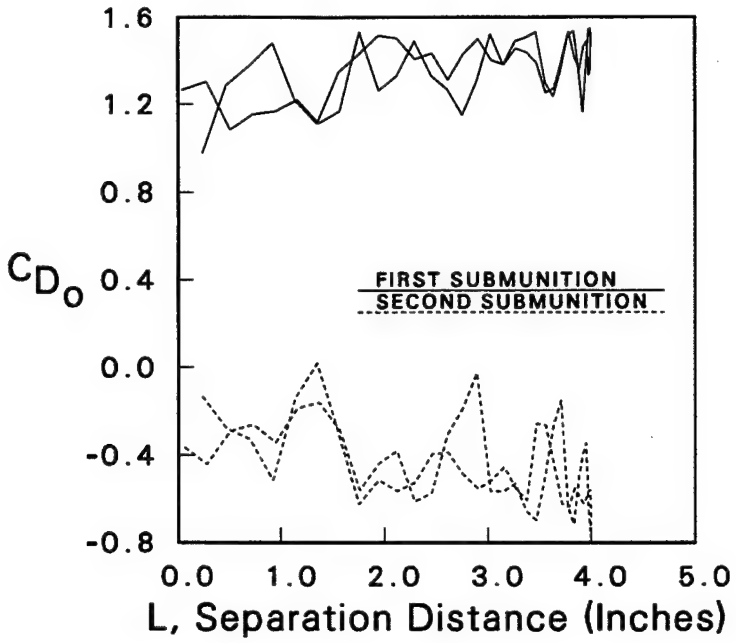

Figure 13. Drag coefficient, M = 0.80, α = 0, V_s = 15 ft/s.

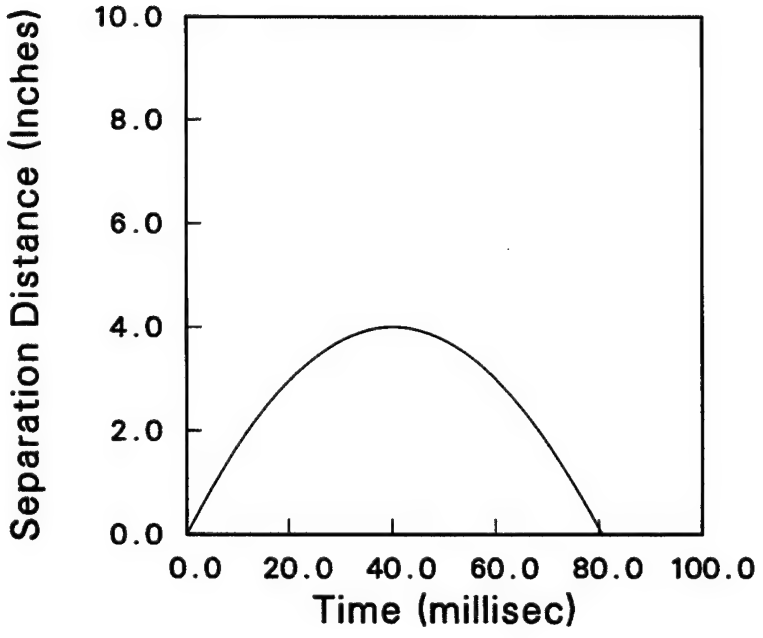

Figure 14. Separation distance vs. time, M = 0.80, α = 0, V_s = 15 ft/s.

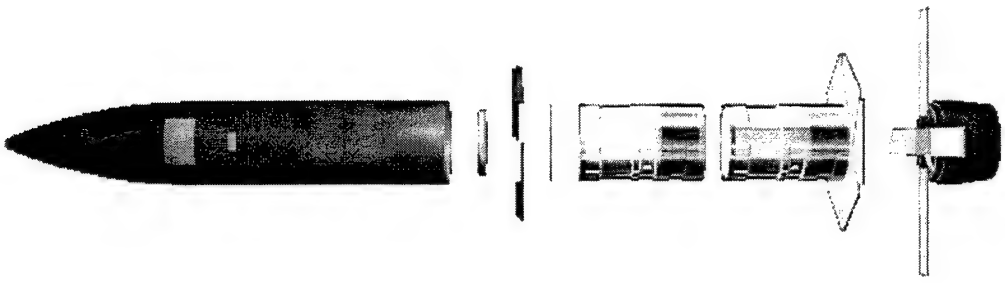

Figure 15. Improved design for SADARM projectile.

Chimera composite overset grid approach was then used to numerically model this experimental, time-dependent separation process. Figure 16 shows the Mach number contours for the submunitions at three points in time (9, 78, and 117 ms) after separation began. As seen in this figure, the second submunition is completely submerged in the wake of the first submunition at 9 ms and begins to separate out from this wake at a later time. The added drag takes effect at about 35 ms of flight. The second submunition is initially seen to separate and then continues to separate (does not come back). The drag coefficient for the submunitions is shown in Figure 17 as a function of the separation distance. The drag for the first submunition is again positive, whereas initially before the drag devices are employed, the second submunition experiences negative drag up to a separation distance of about 8 inches. The drag for the first submunition decreases, and the drag for the second submunition increases from that time on until a separation distance of 20 inches is reached. Although drag fluctuates somewhat, the mean stays at the same value. Figure 18 shows the separation distance as a function of time for this case. As seen here, the separation distance increases with time up to 40 ms. It is seen to level out around 40 ms, and then begins to increase again. The separation distance is clearly seen to increase from that point on, and the two submunitions never come back together. Subsequently, a flight test was conducted. The computed results are compared in this figure with the available experimental data [12] shown in shaded circles and are found to be in good agreement.

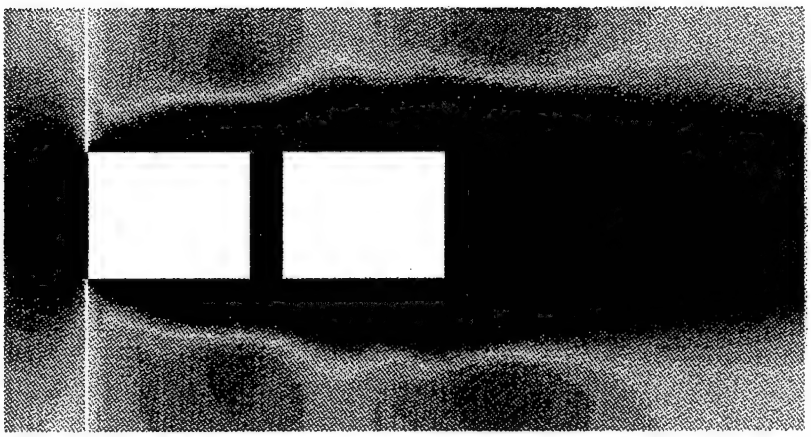

Time = 9.1 ms

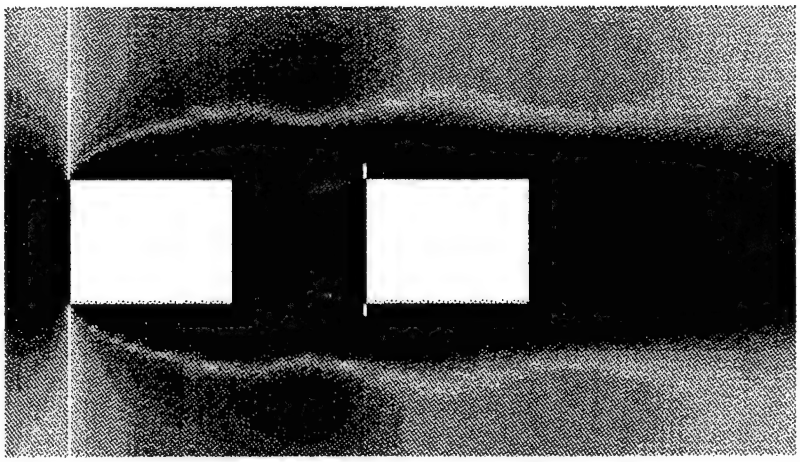

Time = 78 ms

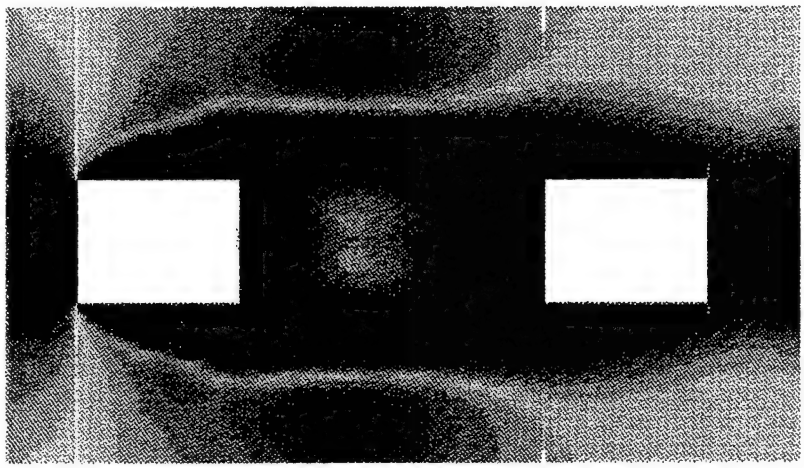

Time = 117 ms

Figure 16. Mach contours, M = 0.80, α = 0, V_s = 15 ft/s with added drag.

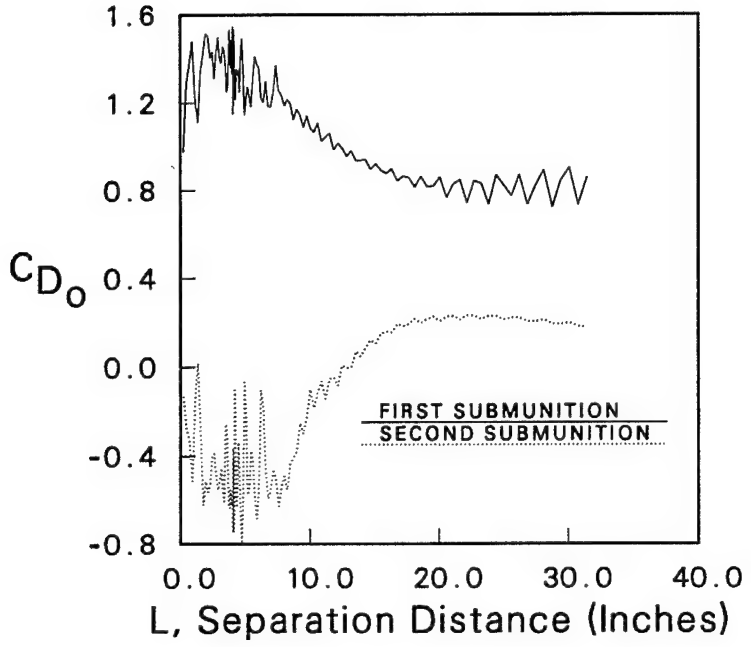

Figure 17. Drag coefficient, M = 0.80, α = 0, V_s = 15 ft/s with added drag.

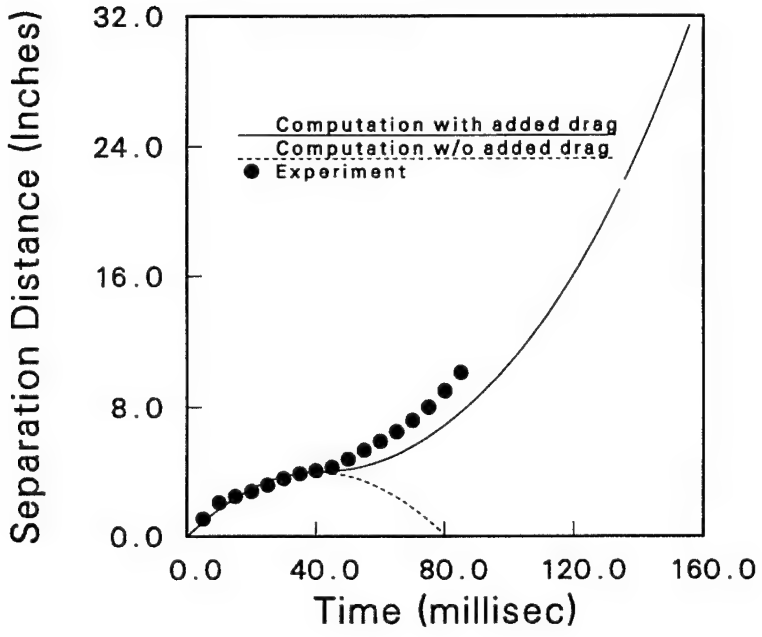

Figure 18. Separation distance vs. time, M = 0.80, α = 0, V_s = 15 ft/s with added drag.

5. CONCLUDING REMARKS

A computational study has been undertaken to compute the time-dependent separation of two cylindrical submunitions in motion. Flow-field computations have been performed at the low transonic Mach number $M_\infty = 0.80$ and angle of attack $\alpha = 0.0°$ using an unsteady, zonal F3D Navier-Stokes code and the Chimera composite grid discretization technique. The computed results show the qualitative features of the wake flow field for both submunitions for three different cases. The predicted flow field over the submunitions was found to undergo significant changes as the submunitions separated from each other. For initial separation velocities of both 5 ft/s and 15 ft/s, the second submunition experiences negative drag for the dynamic case at all times. In both cases, the separation distance increases with time initially until a peak is reached and then decreases until the two submunitions come back and collide. Time-dependent computations were also performed to simulate another case where drag devices were employed after 35 ms of flight, with an initial velocity of 15 ft/s. Comparison of the computed results for this case have been made with available experimental results, and computed separation distances were found to be in good agreement with the experimental results. Both numerical and experimental results show continued separation of the submunitions and thus no collisions for this case.

This work represents a major increase in capability for determining the aerodynamics of multibody configurations and indeed has been successfully applied to the SADARM program. It has resulted in savings of time and dollars and led to the successful March 1995 Defense Acquisition Board action that resulted in low-rate production approval for SADARM. The complex physics and fluid dynamics structure of the aerodynamic interference for the SADARM multibody problem has, for the first time, been uniquely identified and could not have been accomplished without the computational fluid dynamics (CFD) techniques developed in this research effort. This developed technology is additionally applicable to other Army problems such as time-dependent sabot separation for kinetic energy (KE) rounds, segmented rods, multiple launch rocket systems (MLRS), parachute clusters, submunition dispersal, and maneuvering projectiles. The coupling of the fluid dynamic solution and rigid-body motion is a

major advance and a significant accomplishment that eliminates the need for simplifying assumptions and provides a more accurate physically based simulation. These physically based simulations reveal aerodynamic flow-field details not available from experiments, screen new concepts/designs, and minimize expensive flight tests. It is hoped that this work and others like it will create a change from the test-simulate-test environment to the simulate-test-simulate environment.

6. REFERENCES

1. Sahu, J., C. J. Nietubicz, and J. L. Steger. "Navier-Stokes Computations of Projectile Base Flow With and Without Base Injection." AIAA Journal, vol. 23, no. 9, pp. 1348–1355, September 1985.

2. Sahu, J. "Computations of Supersonic Flow Over a Missile Afterbody Containing an Exhaust Jet." AIAA Journal of Spacecraft and Rockets, vol. 24, no. 5, pp. 403–410, September–October 1987.

3. Sahu, J. "Numerical Computations of Transonic Critical Aerodynamic Behavior." AIAA Journal, vol. 28, no. 5, pp. 807–816, May 1990 (also see BRL-TR-2962, U.S. Army Ballistic Research Laboratory, Aberdeen Proving Ground, MD, December 1988).

4. Sahu, J., and C. J. Nietubicz. "Application of Chimera Technique to Projectiles in Relative Motion." ARL-TR-590, U.S. Army Research Laboratory, Aberdeen Proving Ground, MD, October 1994.

5. Steger, J. L., F. C. Dougherty, and J. A. Benek. "A Chimera Grid Scheme." In "Advances in Grid Generation," K. N. Ghia and U. Ghia, eds., ASME FED-5, June 1983.

6. Benek, J. A., T. L. Donegan, and N. E. Suhs. "Extended Chimera Grid Embedding Scheme With Application to Viscous Flows." AIAA Paper No. 87-1126-CP, 1987.

7. Buning, P. G., I. T. Chiu, S. Obayashi, Y. M. Rizk, and J. L. Steger. "Numerical Simulation of the Integrated Space Shuttle Vehicle in Ascent." AIAA Atmospheric Flight Mechanics Conference, August 1988.

8. Meakin, R. L., and N. Suhs. "Unsteady Aerodynamic Simulation of Multiple Bodies in Relative Motion." AIAA 9th Computational Fluid Dynamics Conference, AIAA Paper No. 89-1996, June 1989.

9. Pulliam, T. H., and J. L. Steger. "On Implicit Finite Difference Simulations of Three-Dimensional Flow." AIAA Journal, vol. 18, no. 2, pp. 167–169, February 1982.

10. Baldwin, B. S., and H. Lomax. "Thin Layer Approximation and Algebraic Model for Separated Turbulent Flows." AIAA Paper No. 78–257, January 1978.

11. Steger, J. L., S. X. Ying, and L. B. Schiff. "A Partially Flux-Split Algorithm for Numerical Simulation of Compressible Inviscid and Viscous Flows." Proceedings for the Workshop on Computational Fluid Dynamics, Institute of Non-Linear Sciences, University of California, Davis, CA, 1986.

12. Koenig, W., Private Communications. U.S. Army Armament Research, Development, and Engineering Center, Picatinny Arsenal, NJ, 1995.

INTENTIONALLY LEFT BLANK.

NO. OF COPIES	ORGANIZATION
2	DEFENSE TECHNICAL INFORMATION CENTER DTIC DDA 8725 JOHN J KINGMAN RD STE 0944 FT BELVOIR VA 22060-6218
1	HQDA DAMO FDQ DENNIS SCHMIDT 400 ARMY PENTAGON WASHINGTON DC 20310-0460
1	CECOM SP & TRRSTRL COMMCTN DIV AMSEL RD ST MC M H SOICHER FT MONMOUTH NJ 07703-5203
1	PRIN DPTY FOR TCHNLGY HQ US ARMY MATCOM AMCDCG T M FISETTE 5001 EISENHOWER AVE ALEXANDRIA VA 22333-0001
1	PRIN DPTY FOR ACQUSTN HQS US ARMY MATCOM AMCDCG A D ADAMS 5001 EISENHOWER AVE ALEXANDRIA VA 22333-0001
1	DPTY CG FOR RDE HQS US ARMY MATCOM AMCRD BG BEAUCHAMP 5001 EISENHOWER AVE ALEXANDRIA VA 22333-0001
1	ASST DPTY CG FOR RDE HQS US ARMY MATCOM AMCRD COL S MANESS 5001 EISENHOWER AVE ALEXANDRIA VA 22333-0001

NO. OF COPIES	ORGANIZATION
1	DPTY ASSIST SCY FOR R&T SARD TT F MILTON THE PENTAGON RM 3E479 WASHINGTON DC 20310-0103
1	DPTY ASSIST SCY FOR R&T SARD TT D CHAIT THE PENTAGON WASHINGTON DC 20310-0103
1	DPTY ASSIST SCY FOR R&T SARD TT K KOMINOS THE PENTAGON WASHINGTON DC 20310-0103
1	DPTY ASSIST SCY FOR R&T SARD TT B REISMAN THE PENTAGON WASHINGTON DC 20310-0103
1	DPTY ASSIST SCY FOR R&T SARD TT T KILLION THE PENTAGON WASHINGTON DC 20310-0103
1	OSD OUSD(A&T)/ODDDR&E(R) J LUPO THE PENTAGON WASHINGTON DC 20301-7100
1	ARL ELECTROMAG GROUP CAMPUS MAIL CODE F0250 A TUCKER UNIVERSITY OF TX AUSTIN TX 78712
1	DUSD SPACE 1E765 J G MCNEFF 3900 DEFENSE PENTAGON WASHINGTON DC 20301-3900
1	USAASA MOAS AI W PARRON 9325 GUNSTON RD STE N319 FT BELVOIR VA 22060-5582

NO. OF
COPIES ORGANIZATION

1 CECOM
PM GPS COL S YOUNG
FT MONMOUTH NJ 07703

1 GPS JOINT PROG OFC DIR
COL J CLAY
2435 VELA WAY STE 1613
LOS ANGELES AFB CA 90245-5500

1 ELECTRONIC SYS DIV DIR
CECOM RDEC
J NIEMELA
FT MONMOUTH NJ 07703

3 DARPA
L STOTTS
J PENNELLA
B KASPAR
3701 N FAIRFAX DR
ARLINGTON VA 22203-1714

1 SPCL ASST TO WING CMNDR
50SW/CCX
CAPT P H BERNSTEIN
300 O'MALLEY AVE STE 20
FALCON AFB CO 80912-3020

1 USAF SMC/CED
DMA/JPO
M ISON
2435 VELA WAY STE 1613
LOS ANGELES AFB CA 90245-5500

1 US MILITARY ACADEMY
MATH SCI CTR OF EXCELLENCE
DEPT OF MATHEMATICAL SCI
MDN A MAJ DON ENGEN
THAYER HALL
WEST POINT NY 10996-1786

1 DIRECTOR
US ARMY RESEARCH LAB
AMSRL CS AL TP
2800 POWDER MILL RD
ADELPHI MD 20783-1145

NO. OF
COPIES ORGANIZATION

1 DIRECTOR
US ARMY RESEARCH LAB
AMSRL CS AL TA
2800 POWDER MILL RD
ADELPHI MD 20783-1145

3 DIRECTOR
US ARMY RESEARCH LAB
AMSRL CI LL
2800 POWDER MILL RD
ADELPHI MD 20783-1145

ABERDEEN PROVING GROUND

2 DIR USARL
AMSRL CI LP (305)

NO. OF COPIES	ORGANIZATION
1	HQDA ATTN SARD TR MS K KOMINOS WASHINGTON DC 20310-0103
1	HQDA ATTN SARD TR DR R CHAIT WASHINGTON DC 20310-0103
2	USAF WRIGHT AERONAUTICAL LABORATORIES ATTN AFWAL FIMG DR J SHANG MR N E SCAGGS WPAFB OH 45433-6553
3	COMMANDER NAVAL SURFACE WEAPONS CTR ATTN CODE R44 DR F PRIOLO CODE R44 DR A WARDLAW K24 B402 12 DR W YANTA WHITE OAK LABORATORY SILVER SPRING MD 20903-5000
4	DIRECTOR NATIONAL AERONAUTICS AND SPACE ADMINISTRATION LANGLEY RESEARCH CENTER ATTN TECH LIBRARY MR D M BUSHNELL DR M J HEMSCH DR J SOUTH LANGLEY STATION HAMPTON VA 23665
2	INTERFEROMETRICS INC 8150 LEESBURG PIKE ATTN R LARRIVA E L STROBEL VIENNA VA 22180
2	DARPA ATTN DR P KEMMEY DR J RICHARDSON 3701 NORTH FAIRFAX DR ARLINGTON VA 22203-1714

NO. OF COPIES	ORGANIZATION
7	DIRECTOR NASA AMES RESEARCH CENTER ATTN MS 227 8 L SCHIFF MS 258 1 T HOLST MS 258 1 D CHAUSSEE MS 258 1 M RAI MS 258 1 P KUTLER MS 258 1 P BUNING MS 258 1 B MEAKIN MOFFETT FIELD CA 94035
2	USMA DEPT OF MECHANICS ATTN LTC A L DULL M COSTELLO WEST POINT NY 10996
7	COMMANDER US ARMY ARDEC ATTN SMCAR AET A R DEKLEINE C NG R BOTTICELLI H HUDGINS J GRAU S KAHN W KOENIG PICATINNY ARSENAL NJ 07806-5001
1	COMMANDER US ARMY ARDEC ATTN SMCAR CCH V P VALENTI PICATINNY ARSENAL NJ 07806-5001
1	COMMANDER US ARMY ARDEC ATTN SFAE FAS SD M DEVINE PICATINNY ARSENAL NJ 07806-5001
1	COMMANDER NAVAL SURFACE WEAPONS CTR ATTN DR F MOORE DAHLGREN VA 22448

NO. OF COPIES	ORGANIZATION
2	UNIV OF CALIF DAVIS DEPT OF MECH ENGRG ATTN PROF H A DWYER PROF M HAFEZ DAVIS CA 95616
1	AEROJET ELECTRONICS PLANT ATTN D W PILLASCH B170 DEPT 5311 PO BOX 296 1100 WEST HOLLYVALE STREET AZUSA CA 91702
3	SCIENCE AND TECHNOLOGY INC 4001 NORTH FAIRFAX DR NO 700 ATTN DR A GLASSER MR B LOHMAN MR D MAURIZI ARLINGTON VA 22203-1618
3	AIR FORCE ARMAMENT LAB ATTN AFATL/FXA S C KORN B SIMPSON D BELK EGLIN AFB FL 32542-5434
1	MASSACHUSETTS INSTITUTE OF TECHNOLOGY ATTN TECH LIBRARY 77 MASSACHUSETTS AVE CAMBRIDGE MA 02139
1	GRUMANN AEROSPACE CORP AEROPHYSICS RESEARCH DEPT ATTN DR R E MELNIK BETHPAGE NY 11714
2	MICRO CRAFT INC ATTN DR J BENEK NORMAN SUHS 207 BIG SPRINGS AVE TULLAHOMA TN 37388-0370
1	LOS ALAMOS NATIONAL LAB ATTN MR B HOGAN MS G770 LOS ALAMOS NM 87545

NO. OF COPIES	ORGANIZATION
3	DIRECTOR SANDIA NATIONAL LABS ATTN DIV 1554 DR W OBERKAMPF DIV 1554 DR F BLOTTNER DIV 1636 DR W WOLFE ALBUQUERQUE NM 87185
1	NAVAL AIR WARFARE CENTER ATTN D FINDLAY MS 3 BLDG 2187 PATUXENT RIVER MD 20670
1	METACOMP TECHNOLOGIES INC ATTN S R CHAKRAVARTHY 650 S WESTLAKE BLVD SUITE 203 WESTLAKE VILLAGE CA 91362-3804
2	ROCKWELL SCIENCE CENTER ATTN S V RAMAKRISHNAN V V SHANKAR 1049 CAMINO DOS RIOS THOUSAND OAKS CA 91360
1	ADVANCED TECHNOLOGY CTR ARVIN/CALSPAN AERODYNAMICS RESEARCH DEPT ATTN DR M S HOLDEN PO BOX 400 BUFFALO NY 14225
1	PENNSYLVANIA STATE UNIV DEPT OF AEROSPACE ENGRG ATTN DR G S DULIKRAVICH UNIVERSITY PARK PA 16802
1	UNIV OF ILLINOIS AT URBANA CHAMPAIGN DEPT OF MECH AND INDUSTRIAL ENGRG ATTN DR J C DUTTON URANA IL 61801
1	UNIV OF MARYLAND DEPT OF AEROSPACE ENGRG ATTN DR J D ANDERSON JR COLLEGE PARK MD 20742

NO. OF COPIES ORGANIZATION

1 UNIV OF NOTRE DAME
DEPT OF AERONAUTICAL AND
MECH ENGRG
ATTN PROF T J MUELLER
NOTRE DAME IN 46556

1 UNIV OF TEXAS
DEPT OF AEROSPACE ENGRG MECH
ATTN DR D S DOLLING
AUSTIN TX 78712-1055

1 UNIV OF DELAWARE
DEPT OF MECH ENGRG
ATTN DR J MEAKIN
NEWARK DE 19716

1 UNIV OF FLORIDA
DEPT OF ENGRG SCIENCES
COLLEGE OF ENGRG
ATTN PROF C C HSU
GAINESVILLE FL 32611

NO. OF COPIES ORGANIZATION

ABERDEEN PROVING GROUND

27 DIR, USARL
ATTN: AMSRL-WM-P
A HORST
E SCHMIDT
AMSRL-WM-PB
P PLOSTINS
D LYON
M BUNDY
K FANSLER
E FERRY
B GUIDOS
K HEAVEY
H EDGE
V OSKAY
A MIKHAIL
J SAHU
P WEINACHT
AMSRL-WT, J ROCCHIO
AMSRL-WM-PD, B BURNS
AMSRL-WM-PA
G KELLER
M NUSCA
AMSRL-WM-PC, B FORCH
AMSRL-WM-W, C MURPHY
AMSRL-WM-WB, W D'AMICO
AMSRL-WM-TB, R LOTTERO
AMSRL-CI-H, C NIETUBICZ
AMSRL-CI-HC
P COLLINS
D HISLEY
D PRESSEL
W STUREK

2 CDR, ARDEC
ATTN: FIRING TABLES, BLDG 120
R LIESKE
R EITMILLER

INTENTIONALLY LEFT BLANK.

REPORT DOCUMENTATION PAGE

Form Approved
OMB No. 0704-0188

1. AGENCY USE ONLY *(Leave blank)*	2. REPORT DATE	3. REPORT TYPE AND DATES COVERED
	June 1997	Final, Nov 93 - Nov 95

4. TITLE AND SUBTITLE

Computational Modeling of Sense and Destroy Armor (SADARM) Submunition Separation/Collision

5. FUNDING NUMBERS

PR: 1L161102AH43

6. AUTHOR(S)

Jubaraj Sahu, Karen R. Heavey, and Charles J. Nietubicz

7. PERFORMING ORGANIZATION NAME(S) AND ADDRESS(ES)

U.S. Army Research Laboratory
ATTN: AMSRL-WM-PB
Aberdeen Proving Ground, MD 21005-5066

8. PERFORMING ORGANIZATION REPORT NUMBER

ARL-TR-1378

9. SPONSORING/MONITORING AGENCY NAMES(S) AND ADDRESS(ES)

10.SPONSORING/MONITORING AGENCY REPORT NUMBER

11. SUPPLEMENTARY NOTES

12a. DISTRIBUTION/AVAILABILITY STATEMENT

Approved for public release; distribution is unlimited.

12b. DISTRIBUTION CODE

13. ABSTRACT *(Maximum 200 words)*

Sense and Destroy Armor (SADARM) is a high-priority Army program that experienced an initial design flaw, leading to submunition collisions. Computational fluid dynamics (CFD), including Chimera overset technology, has recently been applied to solve this problem. The CFD modeling has provided significant physical insight into the complex unsteady flow field associated with the SADARM submunitions during the separation/ejection process. CFD simulations have predicted that, with the addition of the fins on the trailing submunition, separation will occur, and collisions will be avoided.

14. SUBJECT TERMS

computational aerodynamics, multiple submunitions, time-dependent flows, moving bodies, relative motion, Chimera overset grids, aerodynamic interference, unsteady wake, transonic flows, and aerodynamic drag

15. NUMBER OF PAGES

36

16. PRICE CODE

17. SECURITY CLASSIFICATION OF REPORT	18. SECURITY CLASSIFICATION OF THIS PAGE	19. SECURITY CLASSIFICATION OF ABSTRACT	20. LIMITATION OF ABSTRACT
UNCLASSIFIED	UNCLASSIFIED	UNCLASSIFIED	UL

INTENTIONALLY LEFT BLANK.

USER EVALUATION SHEET/CHANGE OF ADDRESS

This Laboratory undertakes a continuing effort to improve the quality of the reports it publishes. Your comments/answers to the items/questions below will aid us in our efforts.

1. ARL Report Number/Author ARL-TR-1378 (Sahu) Date of Report June 1997

2. Date Report Received _____

3. Does this report satisfy a need? (Comment on purpose, related project, or other area of interest for which the report will be used.) _____

4. Specifically, how is the report being used? (Information source, design data, procedure, source of ideas, etc.) _____

5. Has the information in this report led to any quantitative savings as far as man-hours or dollars saved, operating costs avoided, or efficiencies achieved, etc? If so, please elaborate. _____

6. General Comments. What do you think should be changed to improve future reports? (Indicate changes to organization, technical content, format, etc.) _____

CURRENT ADDRESS

_____
Organization

_____
Name E-mail Name

_____
Street or P.O. Box No.

_____
City, State, Zip Code

7. If indicating a Change of Address or Address Correction, please provide the Current or Correct address above and the Old or Incorrect address below.

OLD ADDRESS

_____
Organization

_____
Name

_____
Street or P.O. Box No.

_____
City, State, Zip Code

(Remove this sheet, fold as indicated, tape closed, and mail.)
(DO NOT STAPLE)

DEPARTMENT OF THE ARMY

OFFICIAL BUSINESS

NO POSTAGE
NECESSARY
IF MAILED
IN THE
UNITED STATES

BUSINESS REPLY MAIL
FIRST CLASS PERMIT NO 0001,APG,MD

POSTAGE WILL BE PAID BY ADDRESSEE

DIRECTOR
US ARMY RESEARCH LABORATORY
ATTN AMSRL WM PB
ABERDEEN PROVING GROUND MD 21005-5066